J Cereb Blood Flow Metab. Author manuscript; available in PMC 2011 June 21.

Published in final edited form as:
J Cereb Blood Flow Metab. 2008 October ; 28(10): 1742–1753. doi:10.1038/jcbfm.2008.56.

Potential use of oxygen as a metabolic biosensor in combination with T2*-weighted MRI to define the ischemic penumbra

Celestine Santosh[1], **David Brennan**[1,5], **Christopher McCabe**[2,5], **I Mhairi Macrae**[2], **William M Holmes**[2], **David I Graham**[1], **Lindsay Gallagher**[2], **Barrie Condon**[1], **Donald M Hadley**[1], **Keith W Muir**[3], and **Willy Gsell**[4,5]

[1]Institute of Neurological Sciences, Southern General Hospital, Glasgow, UK

[2]Glasgow Experimental MRI Centre, Division of Clinical Neuroscience, University of Glasgow, Glasgow, UK

[3]Division of Clinical Neurosciences, Institute of Neurological Sciences, Southern General Hospital, University of Glasgow, Glasgow, UK

[4]Biological Imaging Centre, MRC Clinical Sciences Centre, Imperial College London, Hammersmith Campus, London, UK

Abstract

We describe a novel magnetic resonance imaging technique for detecting metabolism indirectly through changes in oxyhemoglobin:deoxyhemoglobin ratios and T2* signal change during 'oxygen challenge' (OC, 5 mins 100% O_2). During OC, T2* increase reflects O_2 binding to deoxyhemoglobin, which is formed when metabolizing tissues take up oxygen. Here OC has been applied to identify tissue metabolism within the ischemic brain. Permanent middle cerebral artery occlusion was induced in rats. In series 1 scanning ($n = 5$), diffusion-weighted imaging (DWI) was performed, followed by echo-planar T2* acquired during OC and perfusion-weighted imaging (PWI, arterial spin labeling). Oxygen challenge induced a T2* signal increase of 1.8%, 3.7%, and 0.24% in the contralateral cortex, ipsilateral cortex within the PWI/DWI mismatch zone, and ischemic core, respectively. T2* and apparent diffusion coefficient (ADC) map coregistration revealed that the T2* signal increase extended into the ADC lesion (3.4%). In series 2 ($n = 5$), FLASH T2* and ADC maps coregistered with histology revealed a T2* signal increase of 4.9% in the histologically defined border zone (55% normal neuronal morphology, located within the ADC lesion boundary) compared with a 0.7% increase in the cortical ischemic core (92% neuronal ischemic cell change, core ADC lesion). Oxygen challenge has potential clinical utility and, by distinguishing metabolically active and inactive tissues within hypoperfused regions, could provide a more precise assessment of penumbra.

Keywords

diffusion-weighted imaging; MCAO; oxygen challenge; rat brain; stroke; T2*

Correspondence: Professor IM Macrae, Division of Clinical Neuroscience, University of Glasgow, Garscube Estate, Bearsden Road, Glasgow G61 1QH, UK. m.macrae@udcf.gla.ac.uk.
[5]These authors contributed equally to this work.

Disclosure/conflict of interest The authors have no conflict of interest to declare concerning this research.

Supplementary Information accompanies the paper on the Journal of Cerebral Blood Flow & Metabolism website (http://www.nature.com/jcbfm)

Europe PMC Funders Author Manuscripts

Introduction

Treatment options for acute stroke are currently limited to thrombolysis, the incompletely defined interventions of stroke unit care, and early surgical decompression. Anti-platelet therapies reduce the risk of early stroke recurrence. One reason proposed for the failure to translate efficacy of neuroprotective drugs from animal studies to clinical trials was the heterogeneity of stroke pathophysiology, leading to the inclusion of many patients who lacked a biologic substrate for drug action (Muir, 2002). Physiologic brain imaging to define tissue viability, brain perfusion, or metabolic status promises to improve patient selection for current therapies or for clinical trials. For example, when patients were selected using the results of magnetic resonance imaging (MRI) diffusion–perfusion mismatch analysis, intravenous thrombolysis was shown to remain effective up to 6 h after symptom onset, while also having fewer adverse clinical outcomes than the use of structural imaging with computed tomography alone (Köhrmann *et al*, 2006; Schellinger *et al*, 2007). Magnetic resonance imaging mismatch analysis may optimize patient selection for reperfusion therapies up to 9 h after onset while also providing a biomarker for outcome (Hacke *et al*, 2005).

The viability, duration, and the anatomical extent of the ischemic penumbra vary considerably from patient to patient, and are influenced by many factors. Although time since symptom onset correlates broadly with the volume of penumbral tissue, clinical features and structural imaging alone do not identify the extent of penumbra accurately on an individual basis (Marchal *et al*, 1993).

Current physiologic imaging techniques used to identify penumbral tissue include positron emission tomography (PET) and MRI. Using PET, the penumbra is best identified as a metabolically active region with reduced cerebral blood flow (CBF) characterized by an increased oxygen extraction fraction (Baron, 1999; Marchal *et al*, 1993). However, few stroke units have PET facilities that are able to perform ^{15}O experiments. Positron emission tomography imaging is expensive, with low spatial resolution, and radiation exposure limits repeat imaging in individual subjects. Magnetic resonance imaging is increasingly available in major stroke centers and offers both neuroanatomical and physiologic imaging. The mismatch between the perfusion-weighted images (PWI) and injured tissue in which cellular swelling has already occurred, identified on diffusion-weighted imaging (DWI), has been suggested to define the penumbra (Schlaug *et al*, 1999; Donnan and Davis, 2002). This provides only an approximation of potentially salvageable tissue (Kidwell *et al*, 2003). Currently, no single apparent diffusion coefficient (ADC) threshold defines nonviability of tissue (Fiehler *et al*, 2002; Guadagno *et al*, 2004). Indeed, DWI lesions may be partially or even fully reversible when reperfusion occurs within 2 to 3 h in animal models (Mintorovitch *et al*, 1991; Minematsu *et al*, 1992) with similar findings reported in humans (Kidwell *et al*, 2000; Fiehler *et al*, 2002), although there is also the possibility that they may reappear after a few hours or days.

Similarly, the PWI lesion may include tissue with benign oligemia in addition to penumbra and infarct core, even when optimal thresholds (themselves as yet incompletely defined) are applied (Butcher *et al*, 2005). Therefore, DWI/PWI mismatch represents no more than a rough approximation of the penumbra, although one with some clinical utility.

The penumbra *per se* is defined not only as a region of perfusion deficit but also of some remaining metabolic activity. The absence of a marker of tissue metabolism for penumbra definition in current MRI paradigms renders comparability with standard PET findings difficult and leaves interpretation susceptible to the varied approaches used to define the perfusion deficit.

We therefore sought to develop a new MRI technique in which oxygen is used as a metabolic biosensor to detect tissue metabolism. The technique is based on the different magnetic properties of deoxyhemoglobin and oxyhemoglobin in blood (paramagnetic and diamagnetic, respectively). Oxygen is carried in the blood in two forms: when air is breathed (~21% oxygen), a major part of oxygen combines with hemoglobin to generate oxyhemoglobin but a very small amount dissolves in the plasma (paramagnetic free oxygen). When 100% oxygen is breathed (oxygen challenge (OC)), additional oxygen dissolves in the plasma at a rate of 0.003 mL O_2/100 mL of blood per mm Hg PO_2 (Law and Bukwirwa, 1999).

Hemoglobin enters the brain almost entirely in the form of oxyhemoglobin and gives up oxygen to metabolically active tissue to become deoxyhemoglobin. Therefore, detecting deoxyhemoglobin *in vivo* can indicate oxygen utilization and therefore metabolism. Increasing amounts of deoxyhemoglobin (paramagnetic) reduce the T2* signal on a susceptibility-weighted sequence (Turner *et al*, 1991). During an OC, the additional free oxygen circulates in the plasma where it maintains the level of oxyhemoglobin (diamagnetic), either by directly supplying tissue with oxygen or by binding to deoxyhemoglobin. In metabolically active tissue, OC should therefore cause an increase in T2* signal on susceptibility-weighted imaging from the pre-OC baseline (see online Supplementary Figure 1 for an illustration of the basis of the technique). This increase in T2* signal should reflect the amount of oxygen being taken up by the tissue from the blood. At the end of the OC, free unbound O_2 is no longer present to maintain oxyhemoglobin levels and so deoxyhemoglobin levels will increase as blood flows through metabolizing tissue, and the T2* signal will return to the pre-OC baseline. Therefore, the increase in T2*-weighted signal, its maintenance during the OC, and its return back to baseline when the OC is complete should indicate metabolism within the tissue. This paper presents the results of the OC technique in a rodent stroke model.

Materials and methods

Induction of Middle Cerebral Artery Occlusion

All the experiments were performed under license from the UK Home Office and were subject to the Animals (Scientific Procedures) Act, 1986. Two series of experiments were performed and each series consisted of n=5. This was done because the echo-planar T2* sequence provides T2* and has negligible T1 effect. However, image distortion prevents accurate correlation of T2* maps with histopathology. This was achieved in series 2 using a FLASH T2* sequence. Anesthesia was induced (4% to 5% isoflurane, echo-planar T2*, series 1, or halothane, FLASH T2*, series 2) in adult male Sprague–Dawley rats ($311\pm_{23}$ g, mean±s.d., n = 10, Harlan, UK). The animals were tracheotomized, artificially ventilated, and anesthesia maintained (1.5% to 2% of the respective anesthetic) in a mixture of nitrous oxide and oxygen (70:30) during surgery. After surgery, animals were ventilated with air slightly enriched in oxygen (30%) to maintain physiologic stability under anesthesia. Body temperature was continuously monitored through a rectal thermocouple and maintained at 37°C using a water blanket. Polyethylene catheters were placed in both femoral arteries to continuously monitor blood pressure and conduct blood gas analysis. Middle cerebral artery occlusion (MCAO) was achieved by the intraluminal filament technique, using a modified version of Longa *et al* (1989). Physiologic parameters were maintained within the normal physiologic range under anesthesia apart from increased arterial partial pressure of oxygen (PaO_2) during the OC. $PaCO_2$ was kept as constant as possible (35 to 45 mm Hg) to minimize cerebrovascular reactivity.

MRI Data Acquisition and OC

Magnetic resonance imaging data were acquired on a Bruker Biospec 7T/30 cm system equipped with an inserted gradient coil (121 mm ID, 400mT/m) and a 72 mm birdcage resonator. After surgery, animals were placed prone in a rat cradle, with the head restrained using ear and tooth bars to limit movement, and a linear surface receiver coil (2 cm diameter) was placed above the head of the animal.

Series 1 (n = 5)—DWI was performed before the susceptibility-weighted sequence used during the OC. The sequence for the DWI was a single-shot Spin Echo echo-planar imaging (EPI) diffusion-weighted scan (TE: 43 ms; TR: 4,000.3 ms; four averages; matrix: 96×96; field of view (FOV): 25×25 mm; three directions: *x, y*, and *z*; *B* values: 0 and 1,000 secs/mm^2; eight contiguous slices of 1.5 mm thickness). The sequence used to measure T2* changes during the OC was a single-shot gradient echo EPI sequence (TE: 20 ms; TR: 10 secs; matrix: 96×96; FOV: 25×25 mm; eight contiguous slices of 1.5 mm thickness; two averages; temporal resolution: 20 secs; 75 repetitions). A separate pulsed arterial spin-labeling (ASL) sequence (flow-sensitive alternating inversion recovery; Kim, 1995) was performed on a single slice to produce maps of relative CBF (TE: 20 ms; TR: 8 secs; matrix: 80×64; FOV: 32×25.6 mm; slice thickness: 1.5 mm; two averages): 40 pairs of selective and nonselective images were acquired.

Series 2 (n = 5)—The first MRI sequences consisted of a pilot sequence for positioning and a RARE T2 sequence (effective TE: 46.8 ms; TR: 5,000 ms; four averages; matrix: 256×256; FOV: 25×25 mm; 30 contiguous slices of 0.5 mm thickness) to allow selection of histology sections at the same coronal level as the T2* and DWI scans. To coregister MRI T2* statistical maps with histologic sections (revealing the morphologic status of neurons within the ischemic cortex), a second series of experiments were performed using a Flash 2D T2* gradient echo sequence (TE: 21.4 ms; TR: 317.7 ms; matrix: 128×128; FOV: 25×25 mm; eight contiguous slices of 1 mm thickness; temporal resolution: 37.5 secs for each volume; 40 repetitions) to acquire the susceptibility-weighted images. The advantage of this sequence in comparison with the EPI sequence used in the first series is that images are less distorted and can be obtained at higher spatial resolution, making coregistration with histologic sections more accurate. Diffusion-weighted imaging was performed before the susceptibility-weighted sequence used during the OC. The sequence for the DWI was a Spin Echo EPI diffusion-weighted scan (four-shot EPI; TE: 21.8 ms; TR: 4,000.3 ms; three averages; matrix: 96×96; FOV: 25×25 mm; three directions: *x, y*, and *z*; *B* values: 0, 200, 600, 1,200, and 2,000 secs/mm^2; eight contiguous slices of 1 mm thickness), which was conducted in the same plane as the Flash 2D T2* scan.

In both series of experiments, OC was induced during the T2* scan using the paradigm 5 mins 20 secs with 30% oxygen, 5 mins 20 secs with 100% oxygen, and a final rest period of 16 mins with 30% oxygen. Animals were then removed from the magnet and those undergoing FLASH T2* imaging (series 2) were perfusion fixed (see below) under deep anesthesia for quantitative histopathology of the brain.

Perfusion Fixation and Histology

Transcardiac perfusion with heparinized saline was followed by 4% paraformaldehyde in phosphate buffer. The brains were left in the skull in fixative to prevent dark cell change artifacts (Brierley, 1972), removed 24 h later and immersion fixed before being processed and embedded in paraffin wax. Coronal sections of 6 μm thickness were cut on a microtome and mounted on poly-L-lysine-coated slides. The cutting plane of these sections was as close as possible to the coronal imaging plane acquired with MRI. Coronal sections were stained with hematoxylin and eosin to identify the histologic boundaries between ischemic core,

border zone, and normal cortex and to determine the level of neuronal ischemic cell change in regions of interest (ROIs) defined on the basis of neuronal morphology.

MRI Data Analysis

ADC and CBF infarction thresholds for permanent MCAO—Apparent coefficient diffusion maps were generated from the diffusion scans over eight coronal levels throughout the MCA territory and thresholded to 83.5% of the ADC average of the contralateral hemisphere, which has been shown to match most closely the final infarct size in permanent MCAO (Lo *et al*, 1997). T2*-weighted maps were also generated over the same eight coronal slices. Single-slice ASL was performed to generate a relative CBF map, which matched the fifth coronal slice in core MCA territory. The perfusion deficit was determined using a threshold of 57% of the contralateral hemisphere (Meng *et al*, 2004). The ADC and CBF maps were coregistered to identify the PWI/DWI mismatch area (Figure 1A). Time-course T2* data were also generated from the fifth coronal slice (Figure 3) using an ROI size of 0.61 mm^2 containing nine pixels.

Both echo-planar and FLASH T2* maps were analyzed using statistical parametric mapping (SPM). Before the data were analyzed statistically, motion correction and a spatial smoothing filter of 0.4 mm and high-pass filtering (1,700 secs) were applied. The expected time evolution of the T2* signal during the OC was then applied to the data on a voxel-by-voxel basis by applying a general linear model using an uncorrected statistical threshold of $P < 0.005$ (Friston *et al*, 1995). To align the data, DWI, ASL, and Flash 2D data were scaled to their corresponding RARE T2 slices. RARE T2 slices were warped to the corresponding histology image (which was manually segmented and gray-scaled), using second-order nonlinear warping automated image registration (AIR). The warp parameters were then applied to the DWI and Flash 2D results, allowing the imaging results to be compared with the histology. The processed data from the T2* OC, thresholded ADC, and CBF maps were coregistered to (a) locate the boundary on the thresholded ADC maps and the location of the PWI/DWI mismatch (Figure 1) and (b) define ROIs: IC (ischemic core, in the center of the cortical zone of ADC abnormality), MM (PWI/DWI mismatch, ipsilateral cortex with ADC< 83.5% and CBF <57% of contralateral hemisphere), BZ (border zone, within the area displaying ADC< 83.5% contralateral hemisphere and a positive T2* signal change), and NC (normal cortex, homotopic region of the contralateral cortex) (Figures 1A and 1C). All data are presented as mean$\pm_{s.d.}$ unless otherwise indicated.

Histologic Analysis

An experienced neuropathologist (DG) who was ‘blinded’ to the FLASH T2* and ADC maps selected the histology sections that best matched the anatomical MRI scan at the level of the anterior commissure. Identification of the boundaries between ischemic core, border zone, and normal cortex was achieved by studying the neuronal morphology combined with changes in the neuropil in the form of pallor of staining and microvacuolation (see Figure 2). Regions of interest representing ischemic core (where the majority of cells and neuropil showed the irreversible features of ischemic cell change; Figure 2A), four adjacent fields within the watershed, border zone (mixed population of cells with abnormal and normal morphology; Figure 2B), and adjacent normal cortex (normal cell morphology and neuropil; Figure 2C) were identified on each section within cortical layers 3 to 5. These regions were photographed at ×200 magnification with further magnification (×4) during printing, for an assessment of the percentage of neurons displaying either normal morphology or ischemic cell change (Tamura *et al*, 1981). The ROIs were then superimposed onto the processed FLASH T2* OC and ADC maps using automated image registration software (Woods *et al*, 1998). Oxygen challenge T2* signal time-course data from these regions were then extracted.

Statistical Analysis

Physiologic variables before and during OC were analyzed by Student's paired *t*-test. T2* signal changes in different regions of interest were analyzed by one-way analysis of variance followed by Student's *t*-test with a Bonferroni correction. The influence of OC on relative CBF was analyzed by averaging data within each group before OC and during OC, subtracting one from the other and applying a one-sample *t*-test.

Results

Influence of OC on Physiologic Variables

In series 1, OC was performed $154\pm_{74}$ mins (mean±s.d., $n = 5$) after the onset of the MCA occlusion. Physiologic values recorded before and after OC are detailed in Table 1. All physiological variables remained within the normal physiological range during OC except for the expected increase in arterial partial pressure of oxygen during the inhalation of 100% oxygen. PaO_2 increased 3.5-fold during OC ($P < 0.05$). This resulted in an increase of approximately 5% in the oxygen-carrying capacity of plasma, as every mm Hg rise dissolves an extra 0.003 mL O_2/100 mL blood, once hemoglobin is fully saturated (Law and Bukwirwa, 1999). Oxygen challenge also induced a small, statistically significant increase in mean arterial pressure ($P < 0.005$).

ADC, CBF, and Echo-Planar T2* Data from MCA Territory After Stroke (Series 1)

Thresholded ADC maps identified tissue injured by focal ischemia, thresholded ASL maps identified the perfusion deficit, and coregistration revealed the PWI/DWI mismatch area (MM; Figure 1A), which was 16.05±5.44 mm^2 (n=5)

Echo-planar T2* statistical maps revealed the distribution of significant T2* signal change in response to OC (Figure 1B). In all five animals, the hemisphere contralateral to MCAO showed a significant increase in T2* signal intensity during the OC (Figures 1A and 1B, NC, 1.8%±0.68%) whereas regions in the ischemic core displayed no significant change in T2* signal (Figures 1A and 1B, IC, 0.24%±0.42%). Coregistration of ADC, CBF, and T2* statistical maps revealed a positive T2* signal change within the PWI/DWI mismatch zone (Figure 1A, MM, 3.7%±1.4%), which was significantly greater than the T2* signal change recorded in the contralateral cortex (P<0.05). Similarly, the T2* signal change in the ischemic core was significantly smaller than that in the contralateral cortex (P<0.05). Some tissue within the zone of ADC abnormality (outlined in blue, Figure 1C) also displayed a significant increase in T2* signal on OC (BZ 3.5%±2.4%). The time courses of the T2* signal change in NC, BZ, and IC are presented in Figures 3A to 3C. Oxygen challenge did not significantly influence relative CBF in the border zone (change in normalized signal −0.008, 95% CI −0.066 to 0.081, $P = 0.78$) but did induce a small decrease in CBF in the contralateral cortex (−0.10, 95% CI −0.199 to −0.001, $P = 0.048$; Figure 3D).

FLASH T2* Data and Histology (Series 2)

FLASH T2* signal change during OC was similar to that seen with the echo-planar sequence. Experiments were repeated using FLASH T2* to provide an improved image resolution for coregistration with histology sections. Magnetic resonance scanning started 145±24 mins (mean±s.d., n=5) after MCAO and perfusion fixation of the brains was performed under deep anesthesia at 224±4 mins. Histologically derived ROIs (IC, BZ, and N; Figure 4A), chosen following the definition of the boundaries between ischemic core, border zone, and normal cortex, were superimposed onto the processed T2* and ADC maps. Ninety-two percent of neurons displayed ischemic cell change (Table 2) in the ischemic core, which coregistered within the zone of ADC abnormality and displayed a small 0.7% ±2% positive T2* signal change during OC (IC; Figures 4D and 5D). Histopathological

analysis of the border zone showed a gradual decrease in the number of neurons showing ischemic cell change moving from BZ 0 to BZ 3 (Figure 4A and Table 2), which coregistered with abnormal ADC values, and a $4.9\pm_{2.5\%}$ positive T2* signal change (BZ; Figures 4D and 5C).

Regions of interest identifying normal cortical histology (N; Figure 4A) and a homotopic region in the contralateral cortex co-registered with normal ADC values and a positive T2* signal change on OC (3.5%±1.4% and 3%±1.1%, respectively; Figures 5A and 5B).

Discussion

In this paper, we describe a new 'OC' technique, using oxygen as a biosensor to detect tissue oxygen utilization and define the ischemic penumbra. Increased T2* signal, indicative of continuing oxygen utilization, mapped onto the zone of PWI/DWI mismatch and, beyond this, into the ADC lesion, in a recognized rodent stroke model. Histology confirmed the existence of neurons displaying normal morphology within this defined penumbra.

With PWI/DWI mismatch, the current standard technique for identifying penumbra, accuracy in defining the perfusion and diffusion thresholds to predict infarction is crucial but as yet standard thresholds have not been set for either clinical or preclinical imaging. Further, these thresholds vary, depending on the time elapsed since blood vessel occlusion, and for PWI, extracranial stenosis can further complicate accurate determination of the perfusion deficit. In the current series, we used published thresholds calculated for 3 h after stroke in permanent MCAO in rodents (Meng *et al*, 2004; Lo *et al*, 1997) to define the PWI/DWI mismatch but acknowledge that determining in-house thresholds could further improve penumbra definition. The OC technique offers the prospect of significant improvements over PWI/DWI mismatch in defining penumbral tissue by providing information on the remaining metabolism (oxygen uptake).

Basis for the OC technique

The magnetic properties of oxyhemoglobin and deoxyhemoglobin were shown as long ago as 1936 (Pauling and Coryell, 1936). Deoxyhemoglobin is paramagnetic, and water molecules around red blood cells are affected by the local magnetic field distortions because of its presence. This results in a reduction in the T2* value, which can be detected with susceptibility-weighted imaging. Oxyhemoglobin is diamagnetic and has no such effect. Ogawa *et al* (1990) were able to show a magnetic resonance signal change *in vivo* when the relative amounts of oxyhemoglobin and deoxyhemoglobin were altered in the brain and this blood oxygen level-dependent (BOLD) contrast effect has since been used to show brain activation in response to external stimuli (functional MRI; see Kwong *et al*, 1992).

Blood oxygen level-dependent imaging was applied to animal and human stroke for identification of penumbral tissue, but produced limited results. Reductions in BOLD T2 and T2* have been observed in animal models of global and focal ischemia (Kavec *et al*, 2001; Roussel *et al*, 1995) in response to reductions in CBF. Similarly, Geisler *et al* (2006) using BOLD imaging in acute stroke patients reported significant reductions in $T2'$ (quantitative T2* corrected with spin–spin effects) in the ischemic hemisphere, which they assumed was because of increased deoxyhemoglobin and oxygen extraction fraction in the penumbral tissue. $T2'$ signal decreases were evident within the ADC lesion, in regions outside the ADC lesion later progressing to infarction, and in surviving tissue, compared with the unaffected hemisphere, but variability was such that there was no significant difference in $T2'$ between these three ipsilateral ROIs, preventing estimation of a threshold or the clearcut delineation of the penumbral tissue. Detecting changes in deoxyhemoglobin with BOLD imaging therefore does not provide an adequate surrogate marker for active

metabolism. However, providing dynamic information on changes in oxyhemoglobin:deoxyhemoglobin ratios during OC and mapping statistically significant intensity changes in T2*-weighted images allow identification of tissues responding and not responding to OC (Figures 1B and 4B) and make it possible to discriminate metabolizing tissue within penumbra from nonmetabolizing tissue in the ischemic core.

Within normal metabolizing tissues, the increased oxygen delivery during OC will convert deoxyhemoglobin back to oxyhemoglobin, resulting in an increase in the T2*-weighted signal (Supplementary online Figure 1). This signal increase is maintained during OC and the signal returns to baseline after OC (Figures 3A and 5A). In the ischemic core, in our model, there is no restoration of flow and consequently no significant change in T2* signal is evident during OC (Figures 1B, 3C, and 5D). The border zone between core and normal cortex, as defined by the PWI/DWI mismatch (Figure 3B) or histology (Figure 5C), displayed an increased T2* signal compared with normal cortex. Previous 2-deoxyglucose studies suggest penumbra metabolism within the normal range at 2 h after stroke, with loci of hypermetabolism evident on autoradiograms (Belayev *et al*, 1997; Tohyama *et al*, 1998). Although PET studies detect reduced cerebral metabolic rate of oxygen values within the penumbral tissue relative to nonischemic tissue, values are higher than that in the ischemic core and preserved relative to CBF, leading to high oxygen extraction fraction in humans (Furlan *et al*, 1996) and baboons (Giffard *et al*, 2004). Therefore, as penumbral tissue is metabolic but with restricted blood flow and a high oxygen extraction fraction, the higher level of deoxyhemoglobin in the blood should give rise to a more positive T2* signal change during OC. In our study, the penumbral tissue ROI, as defined by PWI/DWI mismatch, did display the greatest change in T2* during OC (3.7%), which supports the possibility that T2* change during OC reflects oxygen extraction fraction.

The boxcar design used in this study provided information on the rise and fall time of the T2*-weighted signal, which will support further optimization of analysis paradigms in future studies. There is a possibility for low-frequency signal drifts to be classed as statistically significant using this design (false positive), because of the low frequency of this boxcar design. Although it is expected that the contribution from drifts will be minimal, future studies will attempt to account for any such drifts.

For an overview of the basis of the OC technique and T2* responses in ischemic core, penumbra, and normal cortex, see Supplementary online Figure 1.

A region of positive T2* signal change was also found within the zone of ADC abnormality (3.4%), in the watershed area of the ipsilateral dorso-lateral cortex (BZ 0 to BZ 3 containing increasing percentages of morphologically normal neurons on histology; Figures 4A and 4D; Table 2). This suggests that some tissue within the ADC lesion is still viable and metabolizing oxygen, and is supported by reports that injured tissue, identified by DWI or ADC maps, has the potential to recover with early reperfusion and may not evolve into an infarct (Mintorovitch *et al*, 1991; Minematsu *et al*, 1992: Kidwell *et al*, 2000; Fiehler *et al*, 2002). Additional studies, incorporating early reperfusion of ischemic tissue, are planned to validate the accuracy of a positive T2* signal in identifying metabolizing tissue capable of recovery. We are also developing the technique further to define the boundaries between penumbral and benign oligemic tissue (destined to recover). This may be possible by combining T2* signal change during OC with a better-defined assessment of the perfusion deficit. Alternatively, as both echo-planar and FLASH sequences revealed T2* signal changes in PWI/DWI mismatch and border zone of a greater magnitude than contralateral and histologically normal ipsilateral cortex, the OC technique may also provide a means of defining the outer boundary of the penumbra, the focus of subsequent OC studies.

Changes in CBF, CBV, tissue oxygenation, and oxidative metabolism can all influence the T2* signal (Ramsay *et al*, 1993; Corfield *et al*, 2001), so it was important to discount the possibility that factors other than tissue metabolism were influencing the signal change during OC. $PaCO_2$ was regularly monitored and maintained within the physiologic range (Table 1) to avoid any influence of CO_2 on CBF. Oxygen challenge induced a small increase in mean arterial pressure and could therefore have increased CBF, if autoregulation was affected in the ischemic hemisphere. However, ASL revealed no increase in CBF in the border zone or contralateral cortex during OC (Figure 3D). The physiologic significance of the reduction in CBF in contralateral cortex requires further investigation given the borderline statistical significance and the fact that CBF was determined on a single slice within the core MCA territory. Future studies on OC and CBF will use multislice CBF maps throughout the brain and parenchymal laser Doppler flowmetry in ROIs.

Previously, Kety and Schmidt (1948) reported a decrease in CBF during hyperoxia in conscious, normoventilating volunteers, later confirmed by Floyd *et al* (2003). Similarly, hyperoxia induced a small decrease in CBF in anesthetized rat (5.6%; Matsuura *et al*, 2001), anesthetized mouse (9%; Shin *et al*, 2007), and non-human primates (9%; Zhang *et al*, 2007). However, ischemic tissue appears to respond differently to hyperoxia and, in two recent animal MCAO studies, extended periods of hyperoxia have been shown to induce a modest increase in CBF in the ipsilateral hemisphere: for example, after ~10 mins of 100% O_2 in a clip-induced distal MCAO model in mice (Shin *et al*, 2007) and after ~120 mins of 100% O_2 in intraluminal filament-induced permanent MCAO in rat (Henninger *et al*, 2007). Importantly, in the Henninger study, with the same species, strain, and stroke model as the current study, there was no evidence of a significant influence of 100% O_2 on CBF over the first 120 mins of 100% O_2.

Ventilation with 100% oxygen can cause a decrease in tissue T1 (Tadamura *et al*, 1997). Therefore, for the FLASH T2* sequence (TR 317 ms), which has a T1 component, a reduction in tissue T1 during OC would result in a positive signal change (Haacke *et al*, 1999) in addition to the increase seen from T2*. This would lead to a component of the response that was unrelated to oxyhemoglobin:deoxyhemoglobin ratios and tissue metabolism. In the EPI sequence (TR 10 secs) however, there is no such effect, as the magnetization is fully relaxed before the next repetition. Hence the EPI sequence was primarily T2* weighted and any signal increase during OC was because of changes in the oxyhemoglobin:deoxyhemoglobin ratio or perfusion. To produce a positive T2* signal change, CBF would have to increase in response to OC, which was not shown in our study.

In a number of animals, positive T2* signal changes were identified in loci within the ipsilateral striatum (Figure 4B), a region normally identified as ischemic core in permanent MCAO models. The distribution of the positive signal change corresponded to the position of the penetrating arterioles arising from the lenticulo-striate branches of the MCA (Scremin, 1995). This finding may be explained by the fact that MCAO was induced by the intraluminal filament method. We speculate that depending on how well the filament occludes the origin of the MCA, it is possible that a small amount of residual flow through these arterioles may occur and be sufficient to maintain metabolism in tissue immediately adjacent to these blood vessels causing a positive T2* signal on OC.

In these first studies, we specifically chose a permanent MCAO model to simplify interpretation of the OC data. However, as mentioned above, further validation of the technique will involve applying the OC technique in models of transient MCAO. In tissues that are reperfused but where there is no remaining tissue metabolism, there should be little or no conversion of oxyhemoglobin to deoxyhemoglobin. During OC, the oxygen not bound to hemoglobin should remain in a free state within the plasma and as this oxygen is

paramagnetic, the T2* signal change should be negative, depending on the concentration of free oxygen. Therefore after reperfusion, we predict that the ischemic core should show a negative T2* signal change during OC, enabling reperfused, nonmetabolic tissue to be differentiated from metabolic tissue. The technique as described in the current paper has a number of limitations, which should, however, be straightforward to resolve. For example, it should be possible to shorten the interval between MCAO and OC to ~60 mins, the size and number of ROIs can be increased, and upgrading to continuous ASL would permit a mismatch volume, rather than an area to be determined for comparison with T2* changes. Partial volume effects and crossmodality comparison with different resolutions remain one of the challenges of this method. The AIR-based method used for coregistration of MRI scans with histology sections depends on the use of data sets that contain similar contrast and signal information. Some error will result from differences between the histology and magnetic resonance scanning data but is expected to be small when compared with plane slice errors. The most significant errors will result from errors in the histology slice plane with respect to the magnetic resonance scanning plane. Imaging planes were selected by staff with knowledge of the histology procedure to minimize these errors. We used a RARE sequence with an in-plane resolution of 97×97 μm to achieve a precise coregistration. The mismatch of resolution between the histology and the BOLD (Flash) sequence was resolved by sampling the same FOV size on the histology sections. The results from this last assessment thus reflect an average over a FOV similar to the voxel size acquired in MRI. The ROI has also been chosen to be in the middle of the mismatch region to limit the partial volume effect that could lead to inhomogeneous tissue in that voxel. To sample the z dimension, the histologic assessment has been performed over three sections chosen to cover the 1 mm MRI slice.

Finally, there is a significant amount of literature on the beneficial influence of hyperoxia on ischemic tissue and its potential to salvage ischemic brain, extend the time window for acute stroke treatment, reduce the frequency of periinfarct depolarizations, induce ischemic tolerance, and enhance poststroke recovery (Singhal, 2007; Shin *et al*, 2007). Magnetic resonance imaging studies in rodent stroke have revealed hyperoxia-induced recovery of ADC values with prolongation of PWI/DWI mismatch and the time window for beneficial reperfusion, and significant reduction in infarct volumes when hyperoxia was commenced within 30 mins of stroke and lasted for at least 105 mins (Singhal *et al*, 2005; Henninger *et al*, 2007). Oxygen challenge used as a diagnostic tool involves only 5 mins of 100% O_2, so it is debatable whether this would influence penumbral fate. However, temporal changes in T2* during and after OC may provide additional important information on tissue viability.

In conclusion, our novel hypothesis, that positive signal changes on T2*-weighted imaging during OC provide an index of metabolism in ischemic tissue, is supported in these first series of experiments by CBF, histologic findings, and comparison with the PWI/DWI mismatch technique. Further studies are required to identify the boundary between penumbral and benign oligemic tissue and to confirm viability of tissue within regions defined as penumbra using OC. If confirmed, this new MRI technique should be able to discriminate between metabolically active and inactive tissues in the ischemic brain, enable serial imaging and thereby provide an alternative and improved means of defining the ischemic penumbra.

Supplementary Material

Refer to Web version on PubMed Central for supplementary material.

Acknowledgments

The authors thank Mr Jim Mullin and Dr Tracy Farr for technical assistance and Dr Lilian Murray for advice on statistical analysis.

This work was supported by a Research Development Grant from the Scottish Funding Council and Research Grants from the MRC and Neurosciences Foundation.

References

Baron JC. Mapping the ischemic penumbra with PET: implications for stroke treatment. Cerebrovasc Dis. 1999; 9:193–201. [PubMed: 10393405]

Belayev L, Zhao W, Busto R, Ginsberg MD. Transient middle cerebral artery occlusion by intraluminal suture: three-dimensional autoradiographic image-analysis of local cerebral glucose metabolism–blood flow interrelationships during ischemia and early recirculation. J Cereb Blood Flow Metab. 1997; 17:1266–80. [PubMed: 9397026]

Brierley, JB. Cerebral hypoxia. In: Blackwood, W.; Corsellis, JAN., editors. Greenfield's neuropathology. 3rd ed. Arnold; London: 1972. p. 43-85.

Butcher KS, Parsons M, MacGregor L, Barber PA, Chalk J, Bladin C, et al. Refining the perfusion–diffusion mismatch hypothesis. Stroke. 2005; 36:1153–9. [PubMed: 15914768]

Corfield DR, Murphy K, Josephs O, Adams L, Turner R. Does hypercapnia-induced cerebral vasodilation modulate the hemodynamic response to neural activation? NeuroImage. 2001; 13:1207–11. [PubMed: 11352626]

Donnan GA, Davis SM. Neuroimaging, the ischemic penumbra, and selection of patients for acute stroke therapy. Lancet Neurol. 2002; 1:417–25. [PubMed: 12849364]

Fiehler J, Foth M, Kucinski T, Knab R, von Bezold M, Weiller C, Zeumer H, Rother J. Severe ADC decreases do not predict irreversible tissue damage in humans. Stroke. 2002; 33:79–86. [PubMed: 11779893]

Floyd TF, Clark JM, Gelfand R, Detre JA, Ratcliffe S, Guvakov D, Lambertsen CJ, Eckenhoff RG. Independent cerebral vasoconstrictive effects of hyperoxia and accompanying arterial hypocapnia at 1 ATA. J Appl Physiol. 2003; 95:2453–61. [PubMed: 12937024]

Friston KJ, Holmes AP, Worsley KJ, Poline JB, Frith C, Frackowiak RSJ. Statistical parametric maps in functional imaging: a general linear approach. Hum Brain Mapp. 1995; 2:189–210.

Furlan M, Marchal G, Viader F, Derlon JM, Baron J-C. Spontaneous neurological recovery after stroke and the fate of the ischemic penumbra. Ann Neurol. 1996; 40:216–26. [PubMed: 8773603]

Geisler BS, Brandhoff F, Fiehler J, Saager C, Speck O, Rother J, Zeumer H, Kuncinski T. Blood oxygen level-dependent MRI allows metabolic description of tissue at risk in acute stroke patients. Stroke. 2006; 37:1778–84. [PubMed: 16741186]

Giffard C, Young AR, Kerrouche N, Derlon J-M, Baron J-C. Outcome of acutely ischemic brain tissue in prolonged middle cerebral artery occlusion: a serial positron emission tomography investigation in the baboon. J Cereb Blood Flow Metab. 2004; 24:495–508. [PubMed: 15129181]

Guadagno JV, Warburton EA, Aigbirhio FI, Smielewski P, Fryer TD, Harding S, Price CJ, Gillard JH, Carpenter TA, Baron JC. Does the acute diffusion-weighted imaging represent penumbra as well as core? A combined quantitative PET/MRI voxel-based study. J Cereb Blood Flow Metab. 2004; 24:1249–54. [PubMed: 15545920]

Haacke, EM.; Brown, RW.; Thompson, MR.; Venkatesan, R., editors. Magnetic resonance imaging: physical principles and sequence design. John Wiley and Sons; New York: 1999. Fast imaging in the steady state; p. 454-7.chapter 18

Hacke W, Albers G, Al-Rawi Y, Bogousslavsky J, Davalos A, Eliasziw M, Fischer M, Furlan A, Kaste M, Lees KR, Soehngen M, Warach S, for the DIAS Study Group. The desmoteplase in acute ischemic stroke trial (DIAS). A Phase II MRI-based 9-h window acute stroke thrombolysis trial with intravenous desmoteplase. Stroke. 2005; 36:66–73. [PubMed: 15569863]

Henninger N, Bouley J, Nelligan JM, Sicard KM, Fisher M. Normobaric hyperoxia delays perfusion/diffusion mismatch evolution, reduces infarct volume and differentially affects neuronal cell death

pathways after suture middle cerebral artery occlusion in rats. J Cereb Blood Flow Metab. 2007; 27:1632–42. [PubMed: 17311078]

Kavec M, Grohn OH, Kettunen MI, Silvennoinen MJ, Penttonen M, Kauppinen RA. Use of spin echo T2 BOLD in the assessment of misery perfusion at 1.5T. MAGMA. 2001; 12:32–9. [PubMed: 11255090]

Kety SS, Schmidt CF. The effects of altered arterial tensions of carbon dioxide and oxygen on cerebral blood flow and cerebral oxygen consumption of normal young men. J Clin Invest. 1948; 27:484–92. [PubMed: 16695569]

Kidwell CS, Alger JR, Saver JL. Beyond mismatch. Evolving paradigms in imaging the ischemic penumbra with multimodal magnetic resonance imaging. Stroke. 2003; 34:2729–35. [PubMed: 14576370]

Kidwell CS, Saver JL, Mattiello J, Starkman S, Vinuela F, Duckwiler G, Gobin YP, Jahan R, Vespa P, Kalafut M, Alger JR. Thrombolytic reversal of acute human cerebral ischemic injury shown by diffusion/perfusion magnetic resonance imaging. Ann Neurol. 2000; 47:462–9. [PubMed: 10762157]

Kim SG. Quantification of relative cerebral blood flow change by flow-sensitive alternating inversion recovery (FAIR) technique: application to functional mapping. Magn Res Med. 1995; 34:293–301.

Köhrmann M, Jüttler E, Fiebach J, Huttner H, Siebert S, Schwark C, Ringleb P, Schellinger P, Hacke W. MRI versus CT-based thrombolysis treatment within and beyond the 3 h time window after stroke onset: a cohort study. Lancet Neurol. 2006; 5:661–7. [PubMed: 16857571]

Kwong KK, Belliveau JW, Chesler DA, Goldberg IE, Weisskoff RM, Poncelet BP, Kennedy DN, Hoppel BE, Cohen MS, Turner R, CHENG H-M, Brady TJ, Rosen BR. Dynamic magnetic resonance imaging of human brain activity during primary sensory stimulation. Proc Natl Acad Sci USA. 1992; 89:5675–9. [PubMed: 1608978]

Law R, Bukwirwa H. The physiology of oxygen delivery. Update Anaesthesia. 1999; 10:1–2.

Lo EH, Pierce AR, Mandeville JB, Rosen BR. Neuroprotection with NBQX in rat focal cerebral ischemia. Effects on ADC probability distribution functions and diffusion–perfusion relationships. Stroke. 1997; 28:439–47. [PubMed: 9040703]

Longa EZ, Weinstein PR, Carlson S, Cummins R. Reversible middle cerebral artery occlusion without craniectomy in rats. Stroke. 1989; 20:84–91. [PubMed: 2643202]

Marchal G, Serrati C, Rioux P, Petit-Taboue MC, Viader F, de la Sayette V, et al. PET imaging of cerebral perfusion and oxygen consumption in acute ischemic stroke: relation to outcome. Lancet. 1993; 341:925–7. [PubMed: 8096267]

Matsuura T, Kashikura K, Kanno I. Hemodynamics of local cerebral flow induced by somatosensory stimulation under normaxia and hyperoxia in rats. Comp Biochem Physiol. 2001; 129:363–72.

Meng X, Fisher M, Shen Q, Sotak CH, Duong TQ. Characterizing the diffusion/perfusion mismatch in experimental focal cerebral ischemia. Ann Neurol. 2004; 55:207–12. [PubMed: 14755724]

Minematsu K, Li L, Sotak CH, Davis MA, Fisher M. Reversible focal ischemic injury demonstrated by diffusion-weighted magnetic resonance imaging in rats. Stroke. 1992; 23:1304–10. [PubMed: 1519287]

Mintorovitch J, Moseley ME, Chileuitt L, Shimizu H, Cohen Y, Weinstein PR. Comparison of diffusion- and T2-weighted MRI for the early detection of cerebral ischemia and reperfusion in rats. Magn Reson Med. 1991; 18:39–50. [PubMed: 2062240]

Muir KW. Heterogeneity of stroke pathophysiology and neuroprotective clinical trial design. Stroke. 2002; 33:1545–50. [PubMed: 12052989]

Ogawa S, Lee TM, Kay AR, Tank DW. Brain magnetic resonance imaging with contrast dependent on blood oxygenation. Proc Natl Acad Sci USA. 1990; 87:9868–72. [PubMed: 2124706]

Pauling L, Coryell C. The magnetic properties of and structure of hemoglobin, oxyhemoglobin and carbon-monoxyhemoglobin. Proc Natl Acad Sci USA. 1936; 22:210–6. [PubMed: 16577697]

Ramsay SC, Murphy K, Shea SA, Friston KJ, Lammertsma AA, Clark JC, Adams L, Guz A, Frackowiak RS. Changes in global cerebral blood flow in humans: effect on regional cerebral blood flow during neural activation task. J Physiol. 1993; 471:521–34. [PubMed: 8120819]

Roussel SA, van Bruggen N, King MD, Gadian DG. Identification of collaterally perfused areas following focal ischemia in rat by comparison of gradient echo and diffusion weighted MRI. J Cereb Blood Flow Metab. 1995; 15:578–86. [PubMed: 7790407]

Schellinger PD, Thomalla G, Fiehler J, Köhrmann M, Molina CA, Neumann-Haefelin T, Ribo M, Singer OC, Zaro-Weber O, Sobesky J. MRI-based and CT-based thrombolytic therapy in acute stroke within and beyond established time windows: an analysis of 1210 patients. Stroke. 2007; 38:2640–5. [PubMed: 17702961]

Schlaug G, Benfield A, Baird AE, Siewert B, Lovblad KO, Parker RA, et al. The ischemic penumbra: operationally defined by diffusion and perfusion MRI. Neurology. 1999; 53:1528–37. [PubMed: 10534263]

Scremin, OU. Cerebral vascular system. In: Paxinos, G., editor. The rat nervous system. 2nd ed. Academic Ltd; London: 1995. p. 3-35.

Shin HK, Dunn AK, Jones PB, Boas DA, Lo EH, Moskowitz MA, Ayata C. Normobaric hyperoxia improves cerebral blood flow and oxygenation, and inhibits peri-infarct depolarizations in experimental focal ischemia. Brain. 2007; 130:1631–42. [PubMed: 17468117]

Singhal AB. A review of oxygen therapy in ischemic stroke. Neurol Res. 2007; 29:173–83. [PubMed: 17439702]

Singhal AB, Dijkuizen RM, Rosen BR, Lo EH. Normobaric hyperoxia reduces MRI diffusion abnormalities and infarct size in experimental stroke. Neurology. 2005; 58:945–52. [PubMed: 11914413]

Tadamura E, Hatabu H, Li W, Prasad PV, Edelman RR. Effect of oxygen inhalation on relaxation times in various tissues J. Mag Reson Imaging. 1997; 7:220–5.

Tamura A, Graham DI, McCulloch J, Teasdale GM. Focal cerebral ischemia in the rat. 1. Description of technique and early neuropathological consequences following middle cerebral artery occlusion. J Cereb Blood Flow Metab. 1981; 1:53–60. [PubMed: 7328138]

Tohyama Y, Sako K, Yonemasu Y. Hypothermia attenuates hyperglycolysis in the periphery of ischemic core in rat brain. Exp Brain Res. 1998; 122:333–8. [PubMed: 9808306]

Turner R, Le Behan D, Chesnicks AS. Echo-planar imaging of diffusion and perfusion. Magn Reson Med. 1991; 19:247–53. [PubMed: 1881311]

Woods RP, Grafton ST, Watson JDG, Sicotte NL, Mazziotta JC. Automated image registration: II. Intersubject validation of linear and nonlinear models. J Comput Assist Tomogr. 1998; 22:153–65. [PubMed: 9448780]

Zhang X, Nagaoka T, Auerbach EJ, Champion R, Zhou L, HU X, Duong TQ. Quantitative basal CBF and CBF fMRI of rhesus monkeys using three-coil continuous arterial spin labeling. NeuroImage. 2007; 34:1074–83. [PubMed: 17126036]

Europe PMC Funders Author Manuscripts

Europe PMC Funders Author Manuscripts

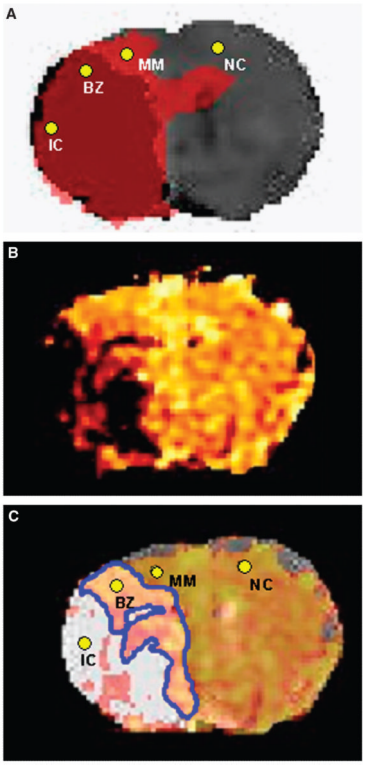

Figure 1.

Series 1. (**A**) Coregistration of thresholded ADC and CBF maps illustrating PWI/DWI mismatch. ROIs used to extract T2* signal changes: IC signifies ischemic core and lies within the dark red region defined by an ADC value <83.5% of the average contralateral value (Lo *et al*, 1997) and blood flow <57% of the average contralateral value (Meng *et al*, 2004); MM signifies mismatch and lies within the adjacent pink region, which defines the PWI/DWI mismatch (ADC>83.5% and CBF<57%); NC signifies contralateral cortex. BZ, representing the ROI within the border zone, is defined in (**C**) as the overlap of positive T2* signal within the region of ADC abnormality. (**B**) Corresponding echo-planar T2* OC statistical map. Colored voxels correspond to a significant T2* signal increase during the inhalation of 100% oxygen; $P<0.005$. (**C**) Coregistration of region of ADC abnormality (ADC<83.5%, white) and T2* map. The region within the ADC lesion boundary that showed a positive T2* change during OC is outlined in blue. ROIs used to extract T2* signal changes: BZ signifies border zone (positive T2* within the ADC lesion boundary). All ROIs have been marked in (**A**) and (**C**) for clarity.

Europe PMC Funders Author Manuscripts

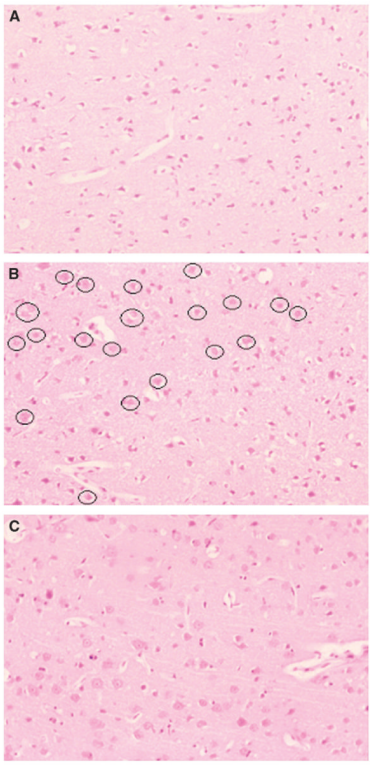

Figure 2.
Histologic photomicrographs of ROI in the dorso-lateral cortex ipsilateral to permanent MCAO from a representative animal. Pictures from hematoxylin- and eosin-stained sections have been captured at ×200 magnification. (**A**) Ischemic core. Note darkly stained triangular neurons that have the features of the ischemic cell process within microvacuolated, pale stained neuropil. (**B**) Border zone. Scattered throughout the ischemic cortex are neurons (circled) that display a normal morphology. (**C**) Normal cortex. Neurons display normal morphology.

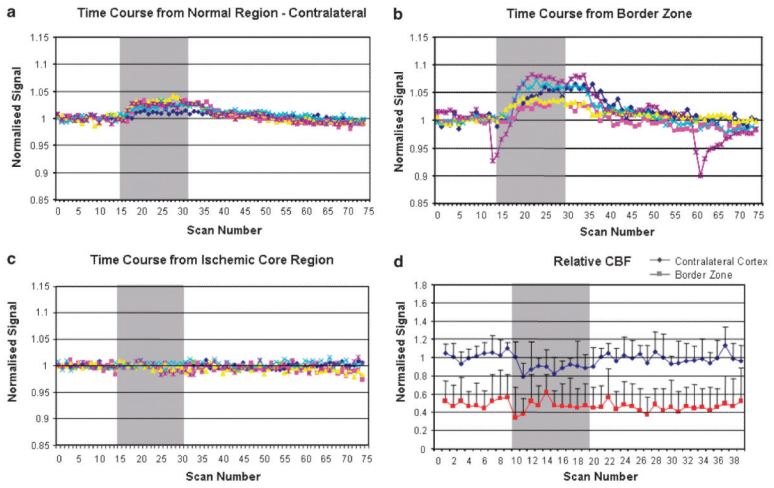

Figure 3.

Series 1: (**A** to **C**) Time course of the echo-planar T2* signal change during OC. (**A**) Contralateral cortex, (**B**) border zone, and (**C**) ischemic core (from ROIs NC, BZ, and IC, respectively, defined in Figure 1C). Graphs display signal intensity changes (%) against scan number for each animal. All data were normalized to the average signal over the 5 mins before OC. (**D**) Relative CBF assessed using arterial spin labeling in the contralateral cortex and border zone. Data (n=5) were normalized to the average signal before OC in the contralateral cortex and are presented as mean$\pm_{\text{s.d.}}$ Change in rCBF during OC was analyzed by a one-sample t-test. OC did not significantly influence CBF in the ipsilateral border zone (−0.008, 95% CI −0.066 to 0.081, P=0.78) but induced a small decrease in CBF in the contralateral cortex (−0.10, 95% CI −0.199 to −0.001, P=0.048). The gray bar the represents period of 100% oxygen inhalation.

Europe PMC Funders Author Manuscripts

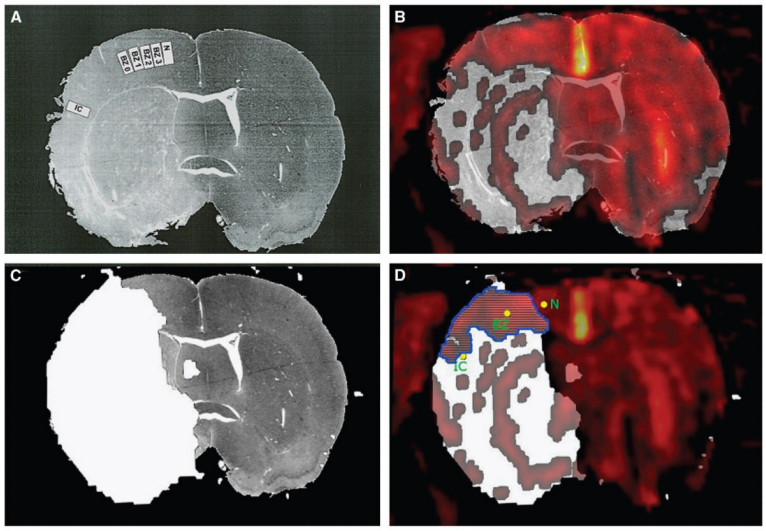

Figure 4.

Series 2: coregistration of histology, FLASH T2* OC map, and ADC map from a representative animal. (**A**) The histologic section displaying adjacent fields where neurons were counted and assessed for features of ischemic cell change by an investigator with no prior knowledge of the MRI maps. BZ, border zones; IC, ischemic core; N, normal cortex. Numerical data are presented in Table 2. (**B**) T2* statistical map overlaid onto the histology section. Colored voxels correspond to a significant T2* signal increase during the inhalation of 100% oxygen; $P<0.005$. (**C**) Localization of region of ADC abnormality, shaded white and defined as tissue displaying an ADC value of <83.5% of the average contralateral value (Lo *et al*, 1997). (**D**) The area of overlap (outlined in blue) between the ADC abnormality (**C**) and positive T2* signal change (**B**). When mapped onto the T2*/ADC maps for each of the five animals, IC always fell within a region showing ADC abnormality and no T2* signal change, BZ fell within the ADC/T2* overlap region or on the boundary on the T2* map between no signal change and a positive signal change, and N fell within the region displaying a normal ADC value and a positive signal change on the T2* map.

Europe PMC Funders Author Manuscripts

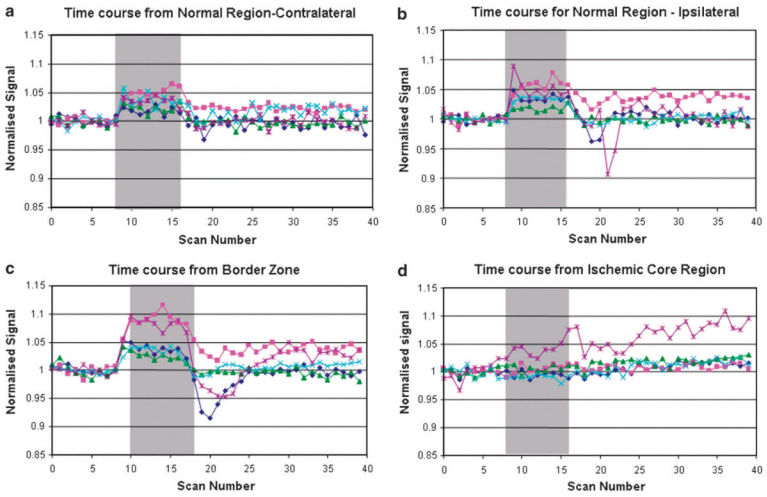

Figure 5.

Series 2: time course of the FLASH T2* signal change during OC. (**A**) Contralateral cortex, (**B**) normal ipsilateral cortex, (**C**) border zone (BZ 0), and (**D**) ischemic core (ROIs defined in Figure 4A). Graphs display signal intensity changes (%) against scan number for each animal. All data were normalized to the average signal over the 5 mins before OC. The gray bar represents the period of 100% oxygen inhalation.

Europe PMC Funders Author Manuscripts

Europe PMC Funders Author Manuscripts

Table 1

Physiological parameters before (prechallenge) and during (challenge) oxygen challenge

	Prechallenge	Challenge
Body temperature (°C)	36.9±0.2	36.8±0.2
Mean arterial blood pressure (mm Hg)	86±9	97±6*
Heart rate (b.p.m.)	381±24	379±23
Blood pH	7.36±0.02	7.34±0.04
PaO_2 (mm Hg)	95.9±11.7	331.6±91.7*
$PaCO_2$ (mm Hg)	37.1±5.5	40.2±1.6

Data are expressed as means±s.d. (series 1, n=5).

*Student's paired t-test revealed a significant increase in mean arterial blood pressure (P<0.005) and PaO_2 (P<0.05) during OC.

Europe PMC Funders Author Manuscripts

Table 2

Neuronal cell counts in ROI displayed in Figure 4A

ROI	Number of morphologically normal neurons per field	Number of neurons displaying ischemic cell change per field	Total number of neurons per field	% of neurons displaying ischemic cell change
Ischemic core (IC)	9.2±4.3	118.4±16.8	127.6±12.6	92±3.9
Border zone (BZ 0)	13.4±3.2	92.2±17.5	105.6±17.8	86±3.7
Border zone (BZ 1)	44.8±15.2	88.6±16.3	133.4±5.5	66±11.8
Border zone (BZ 2)	87.6±15.7	21.8±3.2	109.4±13.0	22±4.8
Border zone (BZ 3)	96.6±13.6	4.8±1.6	101.4±13.4	5±1.9
Normal (N)	94.0±6.0	0.00±0.0	94.0±6.0	0±0.0

Data are presented as mean±s.e.m.; n=5.